

Where Do Deep Fakes Look? Synthetic Face Detection via Gaze Tracking

İlke Demir
Intel Corporation
Santa Clara, CA, USA

Umur Aybars Çiftçi
Binghamton University
Binghamton, NY, USA

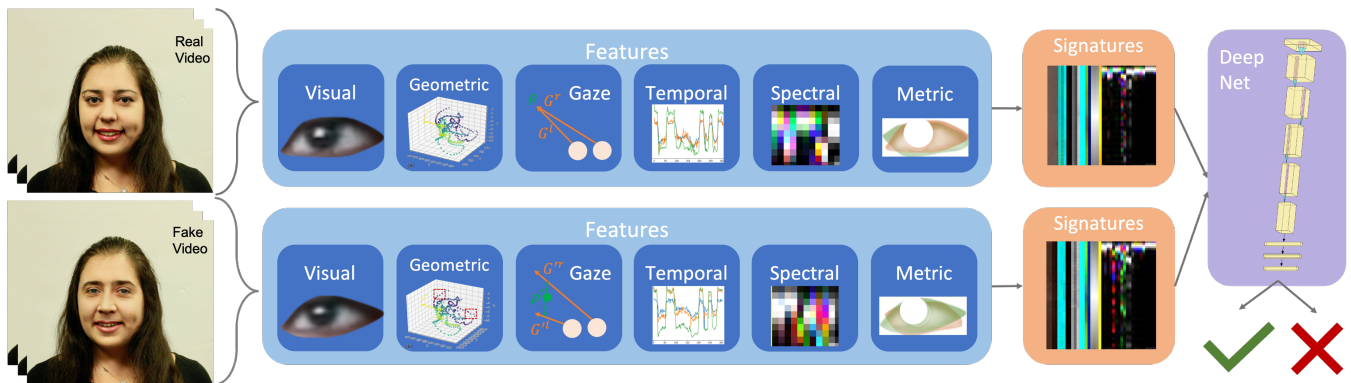


Figure 1: Overview. Our fake detector extracts eye and gaze features from real (top) and fake (bottom) videos. Frame-based features (blue) are converted to temporal signals and spectral densities to forge signatures (orange). Finally, a deep network (purple) predicts authenticity from signatures, and aggregates predictions.

ABSTRACT

Following the recent initiatives for the democratization of AI, deep fake generators have become increasingly popular and accessible, causing dystopian scenarios towards social erosion of trust. A particular domain, such as biological signals, attracted attention towards detection methods that are capable of exploiting authenticity signatures in real videos that are not yet faked by generative approaches. In this paper, we first propose several prominent eye and gaze features that deep fakes exhibit differently. Second, we compile those features into signatures and analyze and compare those of real and fake videos, formulating geometric, visual, metric, temporal, and spectral variations. Third, we generalize this formulation to the deep fake detection problem by a deep neural network, to classify any video in the wild as fake or real. We evaluate our approach on several deep fake datasets, achieving 92.48% accuracy on FaceForensics++, 80.0% on Deep Fakes (in the wild), 88.35% on CelebDF, and 99.27% on DeeperForensics datasets. Our approach outperforms most deep and biological fake detectors with complex network architectures without the proposed gaze signatures. We conduct ablation studies involving different features, architectures, sequence durations, and post-processing artifacts.

Permission to make digital or hard copies of all or part of this work for personal or classroom use is granted without fee provided that copies are not made or distributed for profit or commercial advantage and that copies bear this notice and the full citation on the first page. Copyrights for components of this work owned by others than the author(s) must be honored. Abstracting with credit is permitted. To copy otherwise, or republish, to post on servers or to redistribute to lists, requires prior specific permission and/or a fee. Request permissions from permissions@acm.org.

ETRA '21 Full Papers, May 25–27, 2021, Virtual Event, Germany

© 2021 Copyright held by the owner/author(s). Publication rights licensed to ACM.

ACM ISBN 978-1-4503-8344-8/21/05...\$15.00

<https://doi.org/10.1145/3448017.3457387>

CCS CONCEPTS

• **Computing methodologies** → Scene anomaly detection; **Biometrics**.

KEYWORDS

deep fakes, neural networks, gaze, generative models, fake detection

ACM Reference Format:

İlke Demir and Umur Aybars Çiftçi. 2021. Where Do Deep Fakes Look? Synthetic Face Detection via Gaze Tracking. In *2021 Symposium on Eye Tracking Research and Applications (ETRA '21 Full Papers)*, May 25–27, 2021, Virtual Event, Germany. ACM, New York, NY, USA, 11 pages. <https://doi.org/10.1145/3448017.3457387>

1 INTRODUCTION

With the growth of computational resources and the availability of deep learning models, AI applications thrive on finding new use cases. In particular, generative models invigorate by creating more photorealistic results with each technological advancement. One particular example is in face synthesis domain: The resolution and potent of generated faces have been increasing exponentially since the introduction of Generative Adversarial Networks (GANs) [Goodfellow et al. 2014]. Although realistic synthetic faces are promoted for mixed reality applications, avatars, digital humans, and games; detrimental uses also emerged, such as deep fakes.

Deep fakes are photorealistic synthetic portrait videos generated by deep neural networks, in which the main actor is replaced or reanimated with another person or with a synthetic face. Deep fakes emerged as a novel technique in facial reenactment [Fac

[n.d.]a) and rapidly became a mainstream approach for media manipulation. Consequences are already faced or forecasted, such as impersonation [cnn [n.d.]], celebrity porn [dee [n.d.]], and political misinformation [thr [n.d.]]. Moreover, interdisciplinary groups and governments provided action plans [Chu et al. 2020] and acts [bil [n.d.]] as a precaution for deep fakes.

To combat malicious use of deep fakes, several detection approaches are proposed, mainly categorized as pure deep learning methods and semantic methods. Deep methods classify authenticity only based on the input image/video/audio dataset, without an intermediate representation. Semantic approaches exploit some priors hidden in real or fake data, such as blinks [Li et al. 2018], heart rates [Ciftci et al. 2020a], phoneme-viseme mismatches [Agarwal et al. 2020], or eye reflections [Hu et al. 2020]. First, we observe that the eye-related fake detectors only consider single artifacts of real eyes, as blinks or reflections. Second, by inspecting digital humans in production, we conclude that inconsistent gaze directions, vergence points, and eye symmetries create the "uncanny valley" for synthetic faces. We want to analyze and integrate these variants in a deep fake detector.

In this paper, we first examine the spatial, temporal, and spectral consistency of eyes and gazes in five domains: (i) The visual domain to cover color and shape deformations, (ii) the geometric domain to include characteristics of 3D vergence points and gaze directions, (iii) the temporal domain to assess the consistency of all signals, (iv) the spectral domain to investigate signal and noise correlation, and (v) the metric domain to learn from the deviation of the coupled signals as approximated by the generators. The rest of the paper discloses our classification network that collates described features into a deep fake detector. Our main contributions are listed below.

- We present *the first* holistic analysis on deep fake eyes and gazes; proposing geometric, visual, temporal, spectral, and metric features.
- Based on our analysis, we exploit inconsistencies of synthetic eyes to build a robust deep fake detector.
- We achieve significant accuracies in our experiments on different fake generators, with different visual artifacts, and on unseen deep fakes in the wild; using *only* the proposed eye and gaze features.

We evaluate our approach on four publicly available datasets, namely FaceForensics++ [Rossler et al. 2019], CelebDF [Li et al. 2020b], DeeperForensics [Jiang et al. 2020], and Deep Fakes Dataset [Ciftci et al. 2020a], achieving 92.48%, 88.35%, 99.27% and 80.0% detection accuracies respectively. We conduct ablation studies with different generators, network architectures, sequence lengths, and feature sets. We compare our approach against three biological detectors and six learning-based detectors on three datasets. Finally, we perform experiments including (1) cross validation between dataset splits, (2) cross-dataset evaluations, (3) weighing the contribution of different feature domains, and (4) assessing the robustness against post-generation image manipulation.

2 RELATED WORK

We briefly introduce face synthesis, then delve into detection methods. Although forgery detection is an established domain with

immense literature, we limit our compilation to deep fake detection, especially with biological priors.

2.1 Parametric Face Synthesis

The proliferation of deep generative models enabled realistic face creation and manipulation techniques such as reenactment [Kim et al. 2018; Thies et al. 2016; Wang et al. 2018], attribute or domain manipulation [Choi et al. 2020; He et al. 2017; Nagano et al. 2019], expression molding [Ding et al. 2018], and inpainting [Li et al. 2017b]. In particular, physically grounded models [Li et al. 2020a, 2017a; Saito et al. 2017] generate realistic humans by learning facial parameters. Although there is a few techniques focusing on gaze reenactment [Ganin et al. 2016; Thies et al. 2018], artifacts remain when head is not front-facing and inconsistencies exist between pose and perspective. All of these approaches still lack consistent gazes as (1) their approximations are not accurate at the gaze level, (2) the gaze signatures are not well-replicated in spatial (i.e., misalignment), temporal (i.e., skip frames), and spectral (i.e., noise) domains, and (3) detailed eye models are not encoded in their parametrizations. We aim to use gaze consistency as an authenticity indicator of real videos.

2.2 Fake Detection with Biological Priors

Deep fake detectors either employ complex networks to classify videos without an intermediate representation, or they make use of simpler networks with some semantic interpretation of authenticity signatures or generative residuals. The first family of detectors have limitations such as only processing images [Nguyen et al. 2019; Tariq et al. 2018; Zhang et al. 2017; Zhou et al. 2017] or audio [Korshunov and Marcel 2018], detecting the fakes of specific generators [Afchar et al. 2018; Khodabakhsh et al. 2018; Roy et al. 2018; Tariq et al. 2018] or specific persons [Agarwal et al. 2019], or using small datasets [Li and Lyu 2019; Matern et al. 2019]. We refer the reader to a recent survey [Mirsky and Lee 2020] for the details of each network. The second branch extracts intermediary physiological, biological, or physical signals, then learns the authenticity from their correlations. Such approaches enclose blinks [Jung et al. 2020; Li et al. 2018], head pose [Yang et al. 2019], eye reflections [Hu et al. 2020], heart rates [Ciftci et al. 2020a,b; Conotter et al. 2014], facial attributes [Matern et al. 2019], depth of field [Jeong et al. 2020], eyebrows [Nguyen and Derakhshani 2020], phoneme-viseme mismatches [Agarwal et al. 2020], and affective cues [Mittal et al. 2020]. Most of these approaches need some portion of the skin to be visible, decaying in accuracy under heavy make-up or insufficient illumination. Being invariant to skin reflectance, we aim for a more robust approach under these conditions to outperform and/or complement other fake detectors.

2.3 Gaze-based Fake Detection

Recently, [Li et al. 2018] proposes a robust detector by monitoring irregular blinking patterns successfully. Further investigation of eye traits reveals that the corneal specular highlights for real eyes have strong similarities while those for GAN-synthesized eyes are different. [Hu et al. 2020] introduces a physiological/physical detection method based on that observation. However, this approach

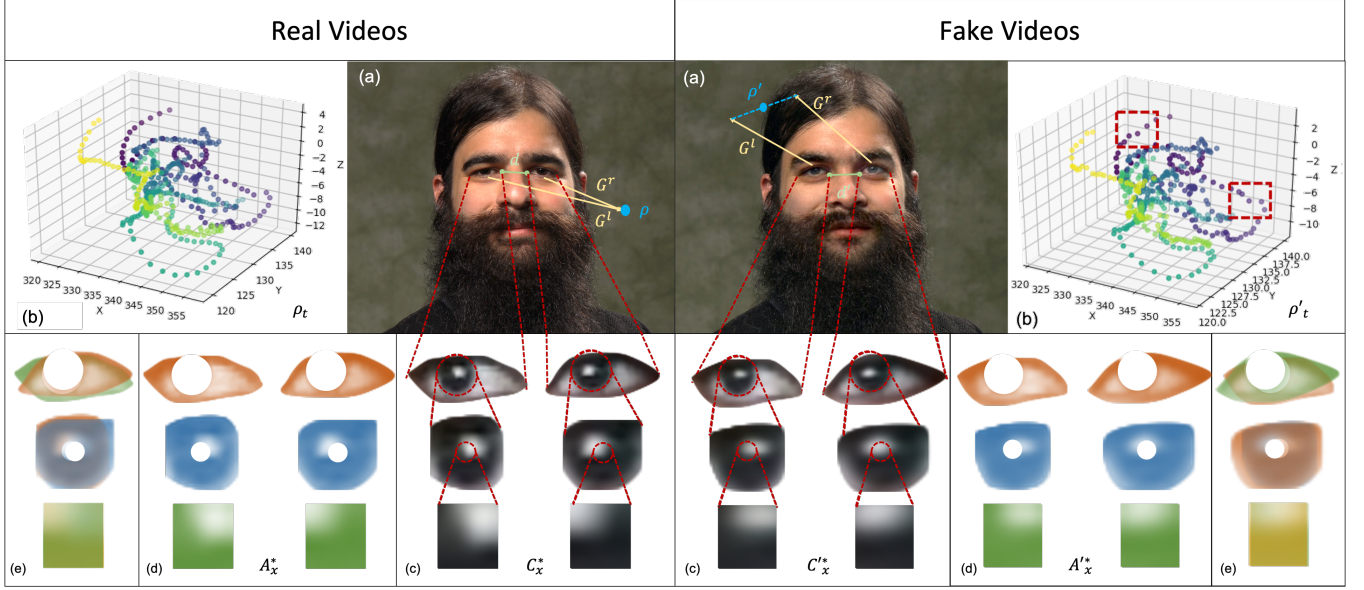


Figure 2: Eye and Gaze Features. Real (left) and fake (right) videos (a), exhibit different geometric (a,b), visual (c,d), and metric (e) features. We draw gaze vectors G^* , 3D gaze points ρ , and pupil distances d on (a).

exposes only one feature of eyes and it is still sensitive to both illumination and pose variations.

In addition to blinking and corneal reflection patterns, gaze is also an important trait to distinguish real and fake videos. Nevertheless, there is no existing work to utilize the eye gaze discrepancy for identifying deep fakes. This paper is to assemble such important but subtle signals to tackle the deep fake detection problem.

To address this issue, essential steps include eye landmark extraction and gaze estimation. In general, eye detection techniques cover (1) shape-based [Hansen and Pece 2005], (2) appearance-based [Hansen and Ji 2010], or (3) hybrid detection [Hansen et al. 2002; Santini et al. 2018]. Gaze estimation methods rely on 2D features [Hansen and Ji 2010] or 3D eye models [Dierkes et al. 2019; Hansen and Ji 2010; Reale et al. 2013]. Recent developments using CNN based gaze estimation has also improved gaze estimation accuracy [Akinyelu and Blignaut 2020; Krafka et al. 2016; Wood et al. 2015; Zhang et al. 2019]. In this paper, we utilize [Baltrusaitis et al. 2018] for extracting eye landmarks, and [Wood et al. 2015] for extracting pupil and iris landmarks in addition to estimating the gaze direction. We also experiment with other approaches and implementations, however they do not provide iris tracking [Zhang et al. 2019], require special software/hardware [Kassner et al. 2014; Zieliski 2007], calibration [Dalmaijer et al. 2014], or configured for mobile [Krafka et al. 2016] or online [Deja 2019] users.

3 3D EYE AND GAZE FEATURES

In order to learn the characteristics of fake gazes, we investigate several eye and gaze features and their contributions to differentiate authenticity. We explore these signals in five subsets, although some features belong to multiple domains. In addition to Figure 1 briefly depicting our proposed features, Figure 2 provides examples for

all of them. We also categorically document all features in Table 7 including their normalizations and contributions to the signatures.

3.1 Visual Features

Visual features V include color C_* and area A_* of eye X_E , iris X_I , and pupil X_P , from left X_*^l and right X_*^r eyes:

$$V = \{C_I^r, C_I^l, C_P^r, C_P^l, A_I^r, A_I^l, A_P^r, A_P^l, A_E^r, A_E^l, |C_I^l - C_I^r|, |C_P^l - C_P^r|\} \quad (1)$$

As shown in Figure 2d, areas correspond to the pixels that are included in the larger region (i.e., iris) but not in the smaller region (i.e., pupil). The color is computed in the CIElab [Connolly and Fleiss 1997] space in order to create illumination independent features, then averaged within the corresponding area (Figure 2c). Assuming that the color difference of iris and pupils from left and right eyes would stay constant (in an illumination invariant color space), we also append color differences (Eqn. 1). Note that we excluded the eye color as it is brittle against illumination and alignment errors.

3.2 Geometric Features

Geometric gaze features L_G include left and right gaze vectors G^l, G^r , 3D gaze point ρ , 3D gaze point approximation $\hat{\rho}$, and the value of the cost function at the approximation δ_ρ . Geometric eye features include the eye distance d , pupil distance d_p , and the difference of areas $|A_*^l - A_*^r|$:

$$L_G = \{G^l, G^r, \rho, \hat{\rho}, \delta_\rho\} \quad (2)$$

$$L_E = \{d, d_p, |A_E^l - A_E^r|, |A_I^l - A_I^r|, |A_P^l - A_P^r|\} \quad (3)$$

We use [Wood et al. 2015] to extract gaze vectors and pupil centers. Then we shoot rays from the pupil centers along the gaze vectors to find their intersection. We aim to optimize for the mid-point of the closes points of the two rays, because it is possible that the rays

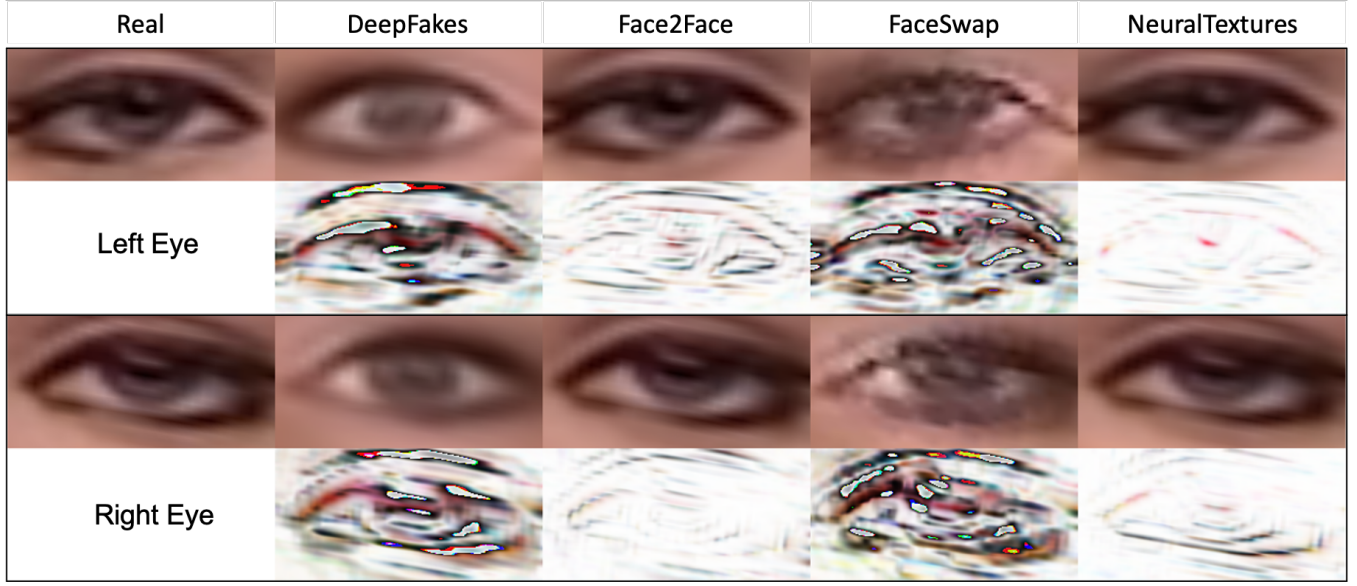


Figure 3: Eye Deformations. Real (first column) and fake (others) eyes are demonstrated to emphasize color differences (even rows) and size differences (i.e., the areas of eye regions in the second column).

are skew lines in 3D. In order to approximate the intersection of two 2D rays in 3D space, we use a least squares optimization with $1e - 08$ threshold. In addition to the approximated 3D gaze point ρ (green points in Figure 2a), we compute the distance between the projections of ρ onto G^l and G_r (orange vectors in Figure 2a), indicated as $\hat{\rho}$ (the green line in fake Figure 2a). We also incorporate the cost at the solution as δ_ρ .

3.3 Temporal Features

As of now, the features we present are computed per frame. However we are less interested in their exact values but more interested in their consistency, therefore we introduce the concept of *sequences*: a fixed ω -length of consecutive frames from a video. We divide all videos into ω length sequences and create signals from the previously defined visual and geometric features, in order to perform our temporal consistency analysis.

$$T = \{V^i, L_G^i, L_E^i\} \text{ such that } i \in [0, \omega] \quad (4)$$

Although ω can be set as a user parameter for detector sensitivity, we experiment with different ω values in Section 6.2.

3.4 Metric Features

In addition to temporal consistency, spatial coherence is an embedded property of authentic videos, especially for symmetries. We employ cross correlation $\phi(*, *)$ of left/right, eye/gaze features to utilize their spatial coherence as an authenticity cue (Figure 2e).

$$M = \{\phi(C_I^l, C_I^r), \phi(C_P^l, C_P^r), \phi(A_I^l, A_I^r), \phi(A_P^l, A_P^r), \phi(A_E^l, A_E^r), \phi(G^l, G^r)\} \quad (5)$$

3.5 Spectral Features

Although we launch our analysis in temporal domain, the environment or the face detection algorithm can introduce noise which deteriorates our temporal features. Thus, we calculate the power spectral density $\Theta(*)$ of all the previously defined signals. Frequency bands play a crucial role in differentiating noise from actual gaze or eye movements.

$$S = \{\Theta(V^i), \Theta(L_G^i), \Theta(L_E^i), \Theta(M)\} \quad (6)$$

In total, we conclude with $40 \times 3 \times \omega$ size signatures with the combination of S and T , all of which are listed in Table 7.

4 GAZE AUTHENTICITY

Having defined our feature space, we explore and analyze the behavior of the predefined features on real and fake gazes. As different generative models create different levels of realism for synthetic faces, they also leave different traces behind [Çiftçi et al. 2020b]. We experiment with several generator outputs [Dee [n.d.]; Fac [n.d.]; Thies et al. 2019, 2016] corresponding to a real sample. For the domains in which the artifacts of different generators are not significantly varying, we discuss them collectively.

4.1 Color and Size Deformations

The visual features V , namely color and size of the eye regions, tend to stay coherent for real videos, even if there is some movement involved. Figure 3 demonstrates close ups of real (first column) and realistic fake (others) eyes of a sample from FF++ dataset. Even for the best fake generator (last column), some of the resolution, striding, or alignment artifacts become visible in close ups. We also emphasize the color differences of those real-fake pairs (even rows) and area changes of regions (i.e., the second column). We delve into those deformations to detect fake videos.

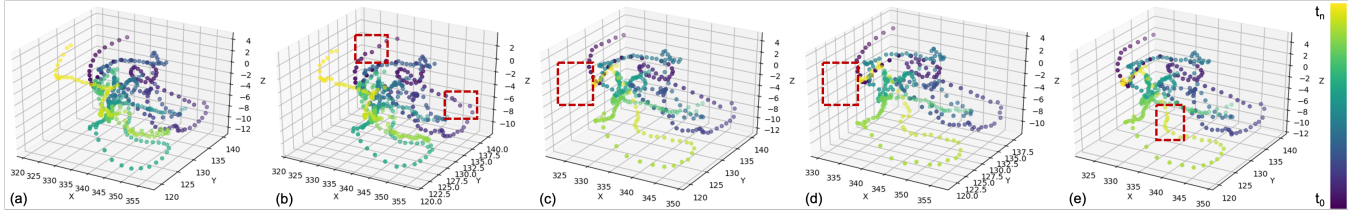


Figure 4: 3D Gaze Points of a real video (a) and its fake counterparts (b-e) are observed for ω frames of a video. Fake gazes exhibit noise (b), miss some saccades (c,d), and have irregular distribution (e). Sample problematic points are boxed in red.

4.2 Geometric Attestation

A visually invisible but computationally powerful way to verify natural gazes is to geometrically validate them. Intuitively, the gaze vectors in real videos converge at a point in 3D space. However, slight deformations of pupil centers or gaze directions may lead to two completely off-plane gaze vectors that never intersect (i.e., Figure 2a fake, or Figure 1 fake). We use vergence points to verify authentic gazes, such that (i) ρ exists and is in front of the face, (ii) $\hat{\rho} = 0$ or is relatively small, and (iii) $\delta_\rho \times \rho$ is close to ρ within the optimization ϵ . Another nice property of ρ_t is that it corresponds to where we naturally look, which has its own form and properties (i.e., smooth pursuits, saccades, etc.) as shown in Figure 4.

4.3 Temporal Consistency

To illustrate temporal consistency of gaze features, we compare the form of 3D gaze points from real (first) and fake (others) versions of a video in Figure 4, color coded by time. In red boxes, we observe that fake gazes exhibit noise (Figure 4b), miss sudden motions (4c,d), and have ragged distributions (4e) compared to real gazes.

Similarly, we show exemplar temporal signals G_t^l , G_t^r , $|A_t^l - A_t^r|_t$, $A_{P_t}^l$, $\hat{\rho}_t$, and ρ_t in Figure 5, of real (green) and fake (blue and orange) videos. Fake gazes may break temporal consistency because of over smoothing (i.e., $G_t^l[0]$, $G_t^r[0]$), or noise (i.e., left-right iris size changes by $30mm^2$), or random distributions (i.e., gaze error).

4.4 Spectral Artifacts

Depending on video resolution, post-processing operations, and illumination; real videos may produce imperfect signals. Those imperfections differ in nature from the generative noise, and the distinctions are best observed in spectral domain. Therefore, we exert power spectral densities of our temporal signals in our analysis, similar to the detection approaches in biological domain [Ciftci et al. 2020a]. Synthetic features produce a richer spectra than reals, as we expect most of our real features to remain constant or coherent. Figure 6 shows the signature blocks, as well as zoom ins to several features, including PSDs of real and fake pupil areas $\Theta(A_{P_t}^*)$ at top right. The colorful bands indicate different spectral densities, so the fake PSD gleams whereas the real PSD contains only a few bands.

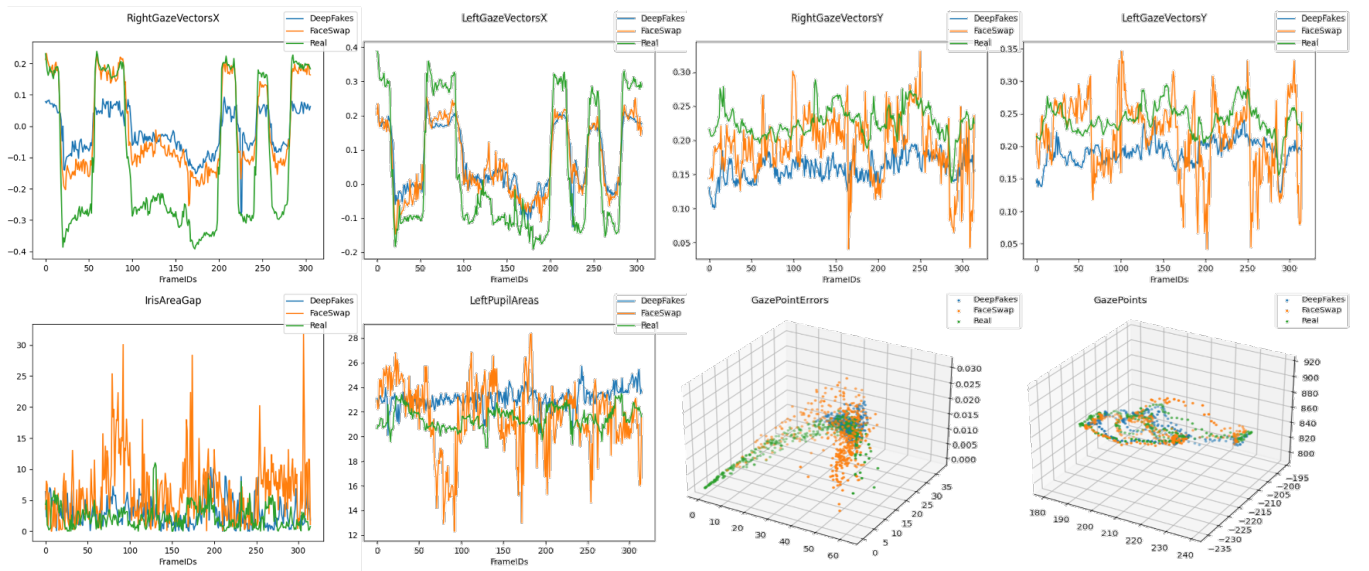


Figure 5: Temporal Signals. Real (green) and fake (orange and blue) signals of (a) $G_t^r[0]$, (b) $G_t^l[0]$, (c) $G_t^r[1]$, (d) $G_t^l[1]$, (e) $|A_t^l - A_t^r|_t$, (f) $A_{P_t}^l$, (g) $\hat{\rho}_t$ and (h) ρ_t . Fake gazes cover less range in (a, b) and they exhibit more noise in (c,d). Fake iris area differences has a $30mm^2$ range in (e) and fake pupil areas can differ by $14mm^2$ in (f).

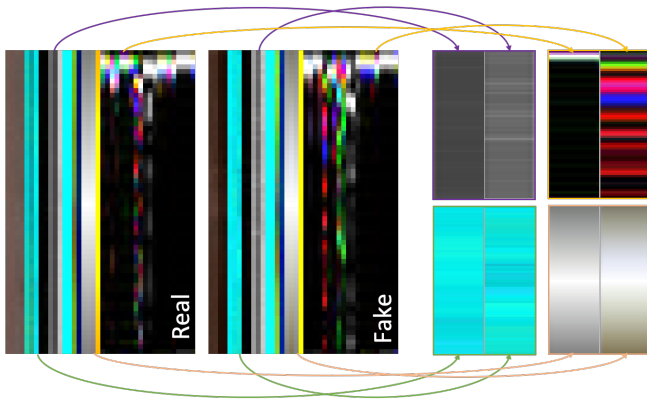


Figure 6: Signatures from real (left block) and fake (mid block) sequences are demonstrated. We zoom into four example signals: (1) Distance of eyes d (first quarter, gray) almost exhibit no change for the real sequence (left), but varies for the fake one (right). (2) Eye areas A_E^* (second quarter, blue) behave similar to (1). (3) PSD of real pupil areas $\Theta(A_{P_i}^*)$ is significantly smaller than the fake $\Theta'(A_{P_i}^*)$ (third quarter, black/colorful). (4) Cross correlation of left and right gaze vectors $\phi(G^L, G^R)$ (fourth quarter) are more uniform for reals than for fakes, as we expect a gray level gradient for the perfect match.

4.5 Symmetry Flaws

Early signs of detecting GAN-generated images were claimed to be asymmetric eyes, ears, and earrings. As the convergence of GANs needs more resources than training other deep networks, results from sooner epochs still exhibit asymmetric eyes as there is no explicit control for coupling eyes. We exploit this shortcoming and experiment with the cross correlation of symmetric pairs of eye and gaze features, with the hypothesis of fake features breaking the symmetry. Our experiments yield that $\Phi = \{\phi(C_P^L, C_P^R), \dots, \phi(G^L, G^R)\}$ (Eqn. 5) increases the detection accuracy.

5 LEARNING AUTHENTICITY BY EYE & GAZE FEATURES

In this section, we build a deep fake detector using our features from Section 3 and our analysis from Section 4.

5.1 Datasets

As our hypothesis of utilizing eye and gaze features for deep fake detection needs to be tested on several deep fake generators, so we need datasets with multiple generators and in the wild samples. For this purpose, we use FaceForensics++ (FF++) [Rossler et al. 2019] dataset with known and Deep Fakes dataset (DF) [Ciftci et al. 2020a] with unknown sources. FF++ dataset includes 1,000 real videos and 4,000 fake videos, generated by four generative models which are FaceSwap [Fac [n.d.]a], Face2Face [Thies et al. 2016], Deepfakes [Dee [n.d.]], and Neural Textures [Thies et al. 2019]. DF dataset, on the other hand, contains 140 in-the-wild deep fakes collected from online sources, thus they are generated by various unknown generators, undergone various post-processing and compression operations. Such deep fakes do not meet any quality standards and their source generative model is unknown, in addition to experiencing occlusion, illumination, etc. artifacts.

We complement our experiments with CelebDF [Li et al. 2020b] (CDF) and DeeperForensics [Jiang et al. 2020] (DFor) datasets to further justify our claim of trusting eye and gaze features as a deep fake litmus. CDF includes 590 real and 5639 fake videos created by their own generative model. DFor contains 50000 real videos of 100 people captured under controlled conditions, and 1000 fake videos, extrapolated to 10000 videos by 10 image distortion algorithms.

5.2 Network Architecture

We treat authenticity detection as a binary classification problem. Our network is made up of three dense layers with 256, 128, and 64 nodes, followed by a last dense layer with 2 nodes. As discussed in the previous section, our features are representative and interpretable, nonetheless our dense architecture may tend to overfit without regularization. Therefore we include batch normalization and dropout layers in between the dense layers to prohibit the network from overfitting. We also add leaky ReLU activations to add non-linearity, and end with a sigmoid activation to obtain the outputs. The detailed model architecture can be observed in Table 8.

5.3 Training Setup

After we extract feature sets S (Eqn. 6) and T (Eqn 4), we normalize all features to be in $[0, 1]$, by shifting and scaling with different values (Table 7). Then we concatenate the processed signals to create our input tensors, or *signatures* (Figure 1, orange boxes), of size $(40, \omega, 3)$. The decomposition of our input tensors are depicted on the left side of Figure 6 and in Table 7. We use the following hyper-parameters determined empirically: Adam optimizer with a learning rate of $1e - 04$, 0.3 dropout probability, batch size of 32, and 0.2 threshold for leaky ReLU layers. We train the models for 100 epochs and validate every 10 epochs.

For training our networks, we gather equal number of real and fake videos from the aforementioned datasets, and create train and test subsets with a 70%-vs-30% split (unless otherwise is noted in the results section). This split is completely random for all datasets and it does not affect the results as demonstrated in Section 6.1.3. Only for CDF, authors provide a predetermined test set of 178 real and 340 fake videos for benchmarking results, thus we use the provided subsets. For DFor, we use 1000 fake videos with no post-processing and 616 real videos with uniform lighting, frontal view, and all expressions. Each train/test pair belongs to one dataset, except cross dataset evaluation in 6.1.3.

5.4 Video Predictions

As our signatures are per sequence (Section 3.3), we need to aggregate sequence predictions from our network into video predictions. Although deep fakes mostly focus on stable faces, they can contain a moving actor, illumination changes, occlusions, and frames without faces. To accommodate for those irregularities, we can trust the

average of the sequence predictions, e.g., if the mean of sequence predictions is closer to fake, we accept the whole video as fake. Another approach is majority voting, where each sequence of a video contributes to a fake or real vote. Instead of counting each sequence as fake or real, we can use the confidence of sequence predictions as a voting score. Or more suitably, we can level with the negative likelihood of sequence predictions contributing to the video prediction. In order to accomplish that, we use the average of log of odds of prediction confidences as the voting scheme:

$$\frac{1}{N_p} \sum_{i < N_p} \log\left(\frac{p_i}{1-p_i}\right) \quad (7)$$

6 RESULTS

We use OpenFace [Baltrusaitis et al. 2018] for eye and face tracking, OpenCV for image processing, SciPy and NumPy for scientific computing, Keras for deep learning, and Matplotlib for visualizations. We train our system on a single NVIDIA GTX 1060 GPU, and a full training loop of 100 epochs takes less than an hour. We continue with our evaluations on different datasets, from different generators, comparisons, validations, experiments, and ablation studies.

6.1 Evaluations and Comparisons

We evaluate our approach on several single and multi-source datasets discussed in Section 5.1 and list our sequence and video accuracy percentages (abbreviated as S. Acc. and V. Acc.) in Table 1. CDF and DFor represent single generator datasets, FF++ is a known multi-generator dataset, and DF is a completely in-the-wild dataset. Our approach detects fakes with 88.35%, 99.27%, 92.48%, and 80% accuracies, respectively. We also evaluate our detector on four known generators of FF++ separately. We observe that for GANs that generate masks without eyes, such as [Thies et al. 2019, 2016], our accuracy is low as expected – they simply do not modify the eyes.

Table 1: Classification accuracies on FF++ generators and single / multi / unknown source datasets.

Source	S. Acc.	V. Acc.
Real	80.36	91.30
DeepFakes	81.02	93.28
Face2Face	58.18	59.69
FaceSwap	80.63	91.62
Neural Tex.	57.46	57.02
CDF [Li et al. 2020b]	85.76	88.35
DFor [Jiang et al. 2020]	95.57	99.27
FF++ [Rossler et al. 2019]	83.12	92.48
DF [Ciftci et al. 2020a]	79.84	80

6.1.1 Comparison with Biological Detectors. In Table 2, we compare our approach against three other biological deep fake detectors built on blinks [Li et al. 2018], which uses only the eye region similar to our approach; head pose, which uses similar information from [Baltrusaitis et al. 2018]; and heart rates [Ciftci et al. 2020a], which uses the information from exposed skin. For a fair comparison, we use the same train and test subsets from FF++ and DF for

all approaches as discussed in Section 5.3, where FF/FS and FF/DF corresponds to FaceSwap and DeepFakes subsets of FF++, respectively. Observing first two rows, blink patterns and head poses are no longer a strong indicator of fake content (50-67%), as generators learn to fake these features. In contrast, heart rates (third row) contain significant authenticity clues similar to our approach (on the average 2.8% better on FF++).

Table 2: Comparison with state-of-the-art biological (1-3) and deep (4-5) detectors on FF and DF. Same data and procedure are used, except results (*) from [Rossler et al. 2019].

Approach	FF/DF	FF/FS	DF
Blink [Li et al. 2018]	67.14	54.15	57.69
Head pose	55.69	50.08	67.85
PPG [Ciftci et al. 2020a]	94.87	95.75	91.07
Inception [Szegedy et al. 2016]	65.5*	54.4*	68.88
Xception [Chollet 2017]	74.5*	70.9*	75.55
Ours	93.28	91.62	80.00

Based on the slightly better results, we investigate and compare [Ciftci et al. 2020a] and our approach. We observe that the failure cases are mutually exclusive, as demonstrated in Figure 7. For false negatives (left half), PPG signals extracted from the skin may be smooth enough to trick [Ciftci et al. 2020a] to classify a fake video as real, however, our approach correctly classifies the same fake video with 84.93% confidence from the eye artifacts (bottom row). For false positives (right half), heavy make up on the skin may deteriorate PPG signals and lead [Ciftci et al. 2020a] to detect a real as fake, however, our approach correctly classifies it due to coherent eye signatures. This motivates us to propose ensemble networks, merging biological detectors working in separate domains to cover for each others' limitations.



Figure 7: Comparison to FakeCatcher [Ciftci et al. 2020a]. A fake video classified as real by [Ciftci et al. 2020a] and as fake by our approach. Artifacts are more visible when zoomed in (bottom). Fake frames from [Rossler et al. 2019].

6.1.2 Comparison with Other Networks. We also compare our approach against six standard deep network architectures, without integrating our eye and gaze features. In Table 3, we listed [Szegedy et al. 2016] and [Chollet 2017] results on three datasets, and in Table 2, we listed [Afchar et al. 2018] and [Tariq et al. 2018] variation results in addition to those of two basic architectures, a three-layer CNN and a ConvLSTM. Our motivation in these comparisons is to justify that the eye and gaze features we formulate contain sufficient information to enable our simple architecture to perform better than deeper and more complex models with more capacity and full frame information.

Table 3: Comparison with other deep fake detectors on DF and FF datasets. Same train/test data and procedure are used for all, except marked results (*) from [Rossler et al. 2019].

Approach	Dataset	Acc.
3-layer CNN	DF	48.88
ConvLSTM	DF	48.83
[Tariq et al. 2018] V3	DF	73.33
[Tariq et al. 2018] ensemble	DF	80.00
MesoNet [Afchar et al. 2018]	FF/DF	87.3*
MesoNet [Afchar et al. 2018]	FF/FS	61.2*

We obtained the results on FF++ from their benchmark, concluding with our approach having 5.98% better accuracy than the second best [Afchar et al. 2018], verifying the contribution of our authenticity formulation. For the results on DF, we use the same setup for training all of the models, namely, the same train/test splits with the same hyper parameters listed in Section 5.3. The only difference is that others are trained with source frames (real or fake) without preprocessing, and ours is trained with our signatures. Despite the in-the-wild setting of DF dataset, our approach outperforms all listed detectors – except having the same accuracy with the complex ensemble network of [Tariq et al. 2018] utilizing full frame information with two order of magnitude more parameters than our model. We emphasize that we *only* input eyes in our fake detector, and still obtain better results, proving the power of the proposed eye and gaze features.

6.1.3 Cross Validation. Giving the benefit of doubt to our random train/test split of datasets, we perform two 5-fold validations with different splits. In the first one, we create five different train-test subset pairs by randomly splitting the aforementioned FF++ dataset as 70%-30%. Then we train and test our approach independently five times on these subsets, with the same procedure discussed in Section 5.3. Five test accuracies have a mean of 90.6% with 1.5% standard deviation.

In the second validation test, we use 80%-20% split to create non-overlapping subsets. In other words, 2000 training videos (1000 fake, 1000 real) are randomly split to mutually exclusive subsets of 400 videos (200 fake, 200 real) as test sets. For each test set, remaining 1600 videos are used for training. Five train and test sessions yield 90.3% mean accuracy with 1.1% standard deviation, validating that our results are independent of the random dataset splits.

Lastly, we conduct a cross dataset evaluation between CDF and DFor datasets. Using the same train and test setup, we train a model

on CDF and test on DFor, then we train a model on DFor and test on CDF. We obtain 80.72% and 73.68% accuracies respectively, which are close to our in-the-wild results.

6.2 Experiments

We summarize the effects of different sequence durations, using several feature sets, under two image-space artifacts.

6.2.1 Sequence Duration. As our method benefits from both temporal and spectral artifacts of continuous signals, such as 3D gaze points in time or frequency bands of iris colors, selection of ω is crucial. We experimentally validate our selection of ω with an ablation study (Table 4), testing different sequence lengths of 16, 32, 64, and 128 on FaceSwap subset of FF++. We monitor that short sequences may contain only noise or missing faces, while long sequences saturate authenticity cues. We can recover from the former during video prediction, but not from the latter one. In short, we conclude on the optimum value of $\omega = 32$ from Table 4.

Table 4: Sequence Durations. We validate the optimum choice of $\omega = 32$ by sequence and video accuracies.

ω	16	32	64	128
S. Acc.	77.72	80.63	79.79	78.60
V. Acc.	89.27	91.62	86.93	85.04

6.2.2 Feature Sets. Next, we train and test our system on FF++ dataset with different feature collections, namely (i) as is, only with (ii) spectral, (iii) temporal, (iv) geometric, (v) visual, and (vi) metric features, (vii-ix) only with raw gaze variants, (x) without metric features, and (xi) without geometric features. All other hyper parameters are held the same. According to Table 5, all five domains of features are contributing to the detection accuracy, however metric features have relatively less importance. Although metric-only results are high (row 6), results without metric features are higher (row 10). We speculate that the size of metric features are relatively smaller in the signature, so they influence the classification less than others, and they can be compensated by other features.

Table 5: Ablation study with and without some of the feature domains from Section 3.

Condition	S. Acc.	V. Acc.
All	83.12	92.48
Spec-only	75.42	84.46
Temp-only	76.39	85.28
Geo-only	79.84	91.82
Visual-only	78.56	88.46
Metric-only	78.52	87.79
Raw gaze	72.88	81.04
Gaze vectors	72.28	80.80
Rows 6 and 7	72.66	81.39
No metric	79.45	88.96
No geometric	79.52	87.98

6.2.3 Postprocessing Artifacts. Generative noise is not the only artifact that deep fakes exhibit, especially in the wild. Post-processing operations, such as compression and resampling, may deteriorate focused signals. In order to test the robustness of our approach, we approximate the post-processing artifacts with two commonly used image processing operations: Gaussian blur and median filtering. All other parameters are kept the same. As enumerated in Table 6, our system is robust against Gaussian and median noise, because effects of such artifacts are minimal for the eye region. As long as the eyes are still visible in videos, features from different domains enforces the detection accuracy to remain the same – i.e., high resolution eyes enable the contributions of geometric features, and low resolution eyes enable the contributions of visual features. This experiment supports the claim that eye/gaze based fake detection is more persistent when other biological fake detectors fail under postprocessing operations, compared to Table 14 of [Ciftci et al. 2020a]. Their accuracy drops by 20.66% under 9x9 Gaussian blur, whereas our accuracy only drops by 0.37%.

Table 6: Robustness. We manually add Gaussian blur and median noise to input videos and evaluate our robustness against such post-processing artifacts.

	Initial	Gaussian Blur			Median Filter		
Kernel	N/A	3x3	7x7	9x9	3x3	7x7	9x9
Accuracy	92.48	89.13	85.88	92.11	91.27	90.77	89.76

7 CONCLUSION AND FUTURE WORK

In this paper, we exhaustively analyze real and fake gazes to answer "Where do Deep Fakes Look?", and morph our findings into a deep fake detector. To the best of our knowledge, our paper conducts the first extensive analysis of deep fake gazes, and it is the first approach to build a detector solely based on holistic eye and gaze features (instead of cherry-picking a few). We evaluate our approach on four datasets, compare against biological and deep detectors, and conduct several ablation studies. As eyes in real videos exhibit natural signatures, which fake ones yet to mimic consistently, we put forward that our visual, geometric, temporal, metric, and spectral features to be integrated to existing fake detectors.

One advantage of our approach is that our signatures are based on authenticity signals instead of generative noise. Blind classifiers without "real" priors are prone to adversarial attacks, as shown in [Hussain et al. 2021] for [Chollet 2017] and [Afchar et al. 2018]. In contrast, fake eye/gaze physics should be spatio-temporally accurate in order to fool our classifier.

On the other hand, as the arms race continues, we also believe that our findings can be used to create better deep fakes with consistent fake gazes. Such synthetic gazes with increased photorealism can be useful for virtual/augmented reality applications, avatars, data augmentation, transfer learning, and controlled learning and testing environments for eye tracking research.

Another future direction is to include gaze classification for our 3D gaze points in order to boost the accuracy of our fake detector. We observe that time-varying 3D gaze points contain much richer biological information that can be utilized if we can interpret them

further – starting from gaze movements such as saccades, fixations, etc. We anticipate that our first step in deciphering fake gazes will lead the way for other deep learning approaches to be inherited for eye or gaze based deep fake detection techniques.

REFERENCES

- [n.d.]. Deep Fakes: A Looming Crisis for National Security, Democracy and Privacy? <https://www.lawfareblog.com/deep-fakes-looming-crisis-national-security-democracy-and-privacy>. Accessed: 2018-11-15.
- [n.d.]. DeepFakes. <https://github.com/deepfakes/faceswap>. Accessed: 2020-03-16.
- [n.d.]a. FaceSwap. <https://github.com/MarekKowalski/FaceSwap>. Accessed: 2020-03-16.
- [n.d.]b. FaceSwap-GAN. <https://github.com/shaoanlu/faceswap-GAN>. Accessed: 2020-03-16.
- [n.d.]. Fake celebrity porn is blowing up on Reddit, thanks to artificial intelligence. <https://www.theverge.com/2018/11/24/16929148/fake-celebrity-porn-ai-deepfake-face-swapping-artificial-intelligence-reddit>. Accessed: 2018-11-15.
- [n.d.]. S.3805 - Malicious Deep Fake Prohibition Act of 2018. <https://www.congress.gov/bill/115th-congress/senate-bill/3805/text>. Accessed: 2020-11-25.
- [n.d.]. When seeing is no longer believing: Inside the Pentagons race against deep-fake videos. <https://www.cnn.com/interactive/2019/01/business/pentagons-race-against-deepfakes/>. Accessed: 2020-11-15.
- Darius Afchar, Vincent Nozick, Junichi Yamagishi, and Isao Echizen. 2018. MesoNet: a Compact Facial Video Forgery Detection Network. In *IEEE International Workshop on Information Forensics and Security (WIFS)*. 1–7. <https://doi.org/10.1109/WIFS.2018.8630761>
- Shruti Agarwal, Hany Farid, Ohad Fried, and Maneesh Agrawala. 2020. Detecting Deep-Fake Videos from Phoneme-Viseme Mismatches. In *Proceedings of the IEEE/CVF Conference on Computer Vision and Pattern Recognition Workshops*. 660–661.
- Shruti Agarwal, Hany Farid, Yuming Gu, Mingming He, Koki Nagano, and Hao Li. 2019. Protecting World Leaders Against Deep Fakes. In *The IEEE Conference on Computer Vision and Pattern Recognition (CVPR) Workshops*.
- Andronicus A Akinyelu and Pieter Bignaut. 2020. Convolutional Neural Network-Based Methods for Eye Gaze Estimation: A Survey. *IEEE Access* 8 (2020), 142581–142605.
- Tadas Baltrusaitis, Amir Zadeh, Yao Chong Lim, and Louis-Philippe Morency. 2018. OpenFace 2.0: Facial Behavior Analysis Toolkit. In *2018 13th IEEE International Conference on Automatic Face Gesture Recognition (FG 2018)*. 59–66. <https://doi.org/10.1109/FG.2018.00019>
- Yunjeon Choi, Youngjung Uh, Jaejun Yoo, and Jung-Woo Ha. 2020. StarGAN v2: Diverse Image Synthesis for Multiple Domains. In *Proceedings of the IEEE Conference on Computer Vision and Pattern Recognition*.
- Francois Chollet. 2017. Xception: Deep Learning With Depthwise Separable Convolutions. In *Proceedings of the IEEE Conference on Computer Vision and Pattern Recognition (CVPR)*.
- David Chu, İlke Demir, Kristen Eichensehr, Jacob G Foster, Mark L Green, Kristina Lerman, Filippo Menczer, Cailin O'Connor, Edward Parson, Lars Ruthotto, et al. 2020. *White Paper: DEEP FAKERY – An Action Plan*. Technical Report <http://www.ipam.ucla.edu/wp-content/uploads/2020/01/Whitepaper-Deep-Fakery.pdf>. Institute for Pure and Applied Mathematics (IPAM), University of California, Los Angeles, Los Angeles, CA.
- Umur Aybars Ciftci, İlke Demir, and Lijun Yin. 2020a. FakeCatcher: Detection of Synthetic Portrait Videos using Biological Signals. *IEEE Transactions on Pattern Analysis & Machine Intelligence (PAMI)* (2020). <https://doi.org/10.1109/TPAMI.2020.3009287>
- Umur Aybars Ciftci, İlke Demir, and Lijun Yin. 2020b. How Do the Hearts of Deep Fakes Beat? Deep Fake Source Detection via Interpreting Residuals with Biological Signals. In *2020 IEEE International Joint Conference on Biometrics (IJCB)*. 1–10. <https://doi.org/10.1109/IJCB48548.2020.9304909>
- Christine Connolly and Thomas Fleiss. 1997. A study of efficiency and accuracy in the transformation from RGB to CIELAB color space. *IEEE Transactions on Image Processing* 6, 7 (1997), 1046–1048. <https://doi.org/10.1109/83.597279>
- Valentina Conotter, Ecaterina Bodnari, Giulia Boato, and Hany Farid. 2014. Physiologically-based detection of computer generated faces in video. In *2014 IEEE International Conference on Image Processing (ICIP)*. 248–252. <https://doi.org/10.1109/ICIP.2014.7025049>
- Edwin S Dalmaijer, Sebastiaan Mathôt, and Stefan Van der Stigchel. 2014. PyGaze: An open-source, cross-platform toolbox for minimal-effort programming of eyetracking experiments. *Behavior research methods* 46, 4 (2014), 913–921.
- Szymon Deja. 2019. GazePointer. <https://sourceforge.net/projects/gazepointer/>.
- Kai Dierkes, Moritz Kassner, and Andreas Bulling. 2019. A Fast Approach to Refraction-Aware Eye-Model Fitting and Gaze Prediction. In *Proceedings of the 11th ACM Symposium on Eye Tracking Research & Applications (Denver, Colorado) (ETRA '19)*. Association for Computing Machinery, New York, NY, USA, Article 23, 9 pages. <https://doi.org/10.1145/3314111.3319819>

- Hui Ding, Kumar Sricharan, and Rama Chellappa. 2018. Exprgan: Facial expression editing with controllable expression intensity. *AAAI* (2018).
- Yaroslav Ganin, Daniil Kononenko, Diana Sungatullina, and Victor Lempitsky. 2016. DeepWarp: Photorealistic Image Resynthesis for Gaze Manipulation. In *Computer Vision – ECCV 2016*, Bastian Leibe, Jiri Matas, Nicu Sebe, and Max Welling (Eds.). Springer International Publishing, Cham, 311–326.
- Ian Goodfellow, Jean Pouget-Abadie, Mehdi Mirza, Bing Xu, David Warde-Farley, Sherjil Ozair, Aaron Courville, and Yoshua Bengio. 2014. Generative Adversarial Nets. In *Advances in Neural Information Processing Systems 27*. Curran Associates, Inc., 2672–2680.
- Dongyoon Han, Jiwon Kim, and Junmo Kim. 2017. Deep Pyramidal Residual Networks. In *Proceedings of the IEEE Conference on Computer Vision and Pattern Recognition (CVPR)*.
- Dan Witzner Hansen, John Paulin Hansen, Mads Nielsen, Anders Sewerin Johansen, and Mikkel B Stegmann. 2002. Eye typing using Markov and active appearance models. In *Sixth IEEE Workshop on Applications of Computer Vision, 2002. (WACV 2002)*. Proceedings, 132–136. <https://doi.org/10.1109/ACV.2002.1182170>
- Dan Witzner Hansen and Qiang Ji. 2010. In the Eye of the Beholder: A Survey of Models for Eyes and Gaze. *IEEE Transactions on Pattern Analysis and Machine Intelligence* 32, 3 (2010), 478–500. <https://doi.org/10.1109/TPAMI.2009.30>
- Dan Witzner Hansen and Arthur E.C. Pece. 2005. Eye tracking in the wild. *Computer Vision and Image Understanding* 98, 1 (2005), 155 – 181. <https://doi.org/10.1016/j.cviu.2004.07.013> Special Issue on Eye Detection and Tracking.
- Zhenliang He, Wangmeng Zuo, Meina Kan, Shiguang Shan, and Xilin Chen. 2017. Arbitrary Facial Attribute Editing: Only Change What You Want. *arXiv:1711.10678* (2017).
- Shu Hu, Yuezun Li, and Siwei Lyu. 2020. Exposing GAN-generated Faces Using Inconsistent Corneal Specular Highlights. *arXiv:2009.11924 [cs.CV]*
- Shehzeen Hussain, Paarth Neekhar, Malhar Jere, Farinaz Koushanfar, and Julian McAuley. 2021. Adversarial Deepfakes: Evaluating Vulnerability of Deepfake Detectors to Adversarial Examples. In *Proceedings of the IEEE/CVF Winter Conference on Applications of Computer Vision (WACV)*, 3348–3357.
- Yonghyun Jeong, Jongwon Choi, Doyeon Kim, Sehyeon Park, Minki Hong, Changhyun Park, Seungjai Min, and Youngjune Gwon. 2020. DoFNet: Depth of Field Difference Learning for Detecting Image Forgery. In *Proceedings of the Asian Conference on Computer Vision (ACCV)*.
- Liming Jiang, Ren Li, Wayne Wu, Chen Qian, and Chen Change Loy. 2020. DeeperForensics-1.0: A Large-Scale Dataset for Real-World Face Forgery Detection. In *CVPR*.
- Tackhyun Jung, Sangwon Kim, and Keecheon Kim. 2020. DeepVision: Deepfakes Detection Using Human Eye Blinking Pattern. *IEEE Access* 8 (2020), 83144–83154. <https://doi.org/10.1109/ACCESS.2020.2988660>
- Moritz Kassner, William Patera, and Andreas Bulling. 2014. Pupil: An Open Source Platform for Pervasive Eye Tracking and Mobile Gaze-based Interaction. In *Adjunct Proceedings of the 2014 ACM International Joint Conference on Pervasive and Ubiquitous Computing (Seattle, Washington) (UbiComp '14 Adjunct)*. ACM, New York, NY, USA, 1151–1160. <https://doi.org/10.1145/2638728.2641695>
- Ali Khodabakhsh, Raghavendra Ramachandra, Kiran Raja, Pankaj Wasnik, and Christoph Busch. 2018. Fake Face Detection Methods: Can They Be Generalized?. In *2018 International Conference of the Biometrics Special Interest Group (BIOSIG)*, 1–6. <https://doi.org/10.23919/BIOSIG.2018.8553251>
- Hyeongwoo Kim, Pablo Garrido, Ayush Tewari, Weipeng Xu, Justus Thies, Matthias Niessner, Patrick Pérez, Christian Richardt, Michael Zollhöfer, and Christian Theobalt. 2018. Deep Video Portraits. *ACM Trans. Graph.* 37, 4, Article 163 (July 2018), 14 pages.
- Pavel Korshunov and Sébastien Marcel. 2018. Speaker Inconsistency Detection in Tampered Video. In *2018 26th European Signal Processing Conference (EUSIPCO)*, 2375–2379. <https://doi.org/10.23919/EUSIPCO.2018.8553270>
- Kyle Krafka, Aditya Khosla, Petr Kellnhofer, Harini Kannan, Suchendra Bhandarkar, Wojciech Matusik, and Antonio Torralba. 2016. Eye Tracking for Everyone. In *Proceedings of the IEEE Conference on Computer Vision and Pattern Recognition (CVPR)*.
- Ruilong Li, Karl Bladin, Yajie Zhao, Chinmay Chinara, Owen Ingraham, Pengda Xiang, Xinglei Ren, Pratusha Prasad, Bipin Kishore, Jun Xing, and Hao Li. 2020a. Learning Formation of Physically-Based Face Attributes. In *Proceedings of the IEEE/CVF Conference on Computer Vision and Pattern Recognition (CVPR)*.
- Tianye Li, Timo Bolkart, Michael J. Black, Hao Li, and Javier Romero. 2017a. Learning a model of facial shape and expression from 4D scans. *ACM Transactions on Graphics, (Proc. SIGGRAPH Asia)* 36, 6 (2017). <https://doi.org/10.1145/3130800.3130813>
- Xiang Li, Shuo Chen, Xiaolin Hu, and Jian Yang. 2019. Understanding the Disharmony Between Dropout and Batch Normalization by Variance Shift. In *Proceedings of the IEEE/CVF Conference on Computer Vision and Pattern Recognition (CVPR)*.
- Yuezun Li, Ming-Ching Chang, and Siwei Lyu. 2018. In Ictu Oculi: Exposing AI Generated Fake Face Videos by Detecting Eye Blinking. *arXiv e-prints*, Article arXiv:1806.02877 (Jun 2018), arXiv:1806.02877 pages. [arXiv:1806.02877 \[cs.CV\]](https://arxiv.org/abs/1806.02877)
- Yijun Li, Sifei Liu, Jimei Yang, and Ming-Hsuan Yang. 2017b. Generative Face Completion. In *IEEE Conference on Computer Vision and Pattern Recognition*.
- Yuezun Li and Siwei Lyu. 2019. Exposing DeepFake Videos By Detecting Face Warping Artifacts. In *The IEEE Conference on Computer Vision and Pattern Recognition (CVPR) Workshops*.
- Yuezun Li, Pu Sun, Honggang Qi, and Siwei Lyu. 2020b. Celeb-DF: A Large-scale Challenging Dataset for DeepFake Forensics. In *IEEE Conf. on Computer Vision and Pattern Recognition (CVPR)*. Seattle, WA, United States.
- Falko Matern, Christian Riess, and Marc Stamminger. 2019. Exploiting Visual Artifacts to Expose Deepfakes and Face Manipulations. In *IEEE Winter Applications of Computer Vision Workshops (WACVW)*, 83–92. <https://doi.org/10.1109/WACVW.2019.00020>
- Yisroel Mirsky and Wenke Lee. 2020. The Creation and Detection of Deepfakes: A Survey. *arXiv preprint arXiv:2004.11138* (2020).
- Trisha Mittal, Uttaran Bhattacharya, Rohan Chandra, Aniket Bera, and Dinesh Manocha. 2020. Emotions Don't Lie: An Audio-Visual Deepfake Detection Method Using Affective Cues. In *Proceedings of the 28th ACM International Conference on Multimedia (Seattle, WA, USA) (MM '20)*. Association for Computing Machinery, New York, NY, USA, 2823?2832. <https://doi.org/10.1145/3394171.3413570>
- Koki Nagano, Huiwen Luo, Zejian Wang, Jaewoo Seo, Jun Xing, Liwen Hu, Lingyu Wei, and Hao Li. 2019. Deep Face Normalization. *ACM Trans. Graph.* 38, 6, Article 183 (Nov. 2019), 16 pages. <https://doi.org/10.1145/3355089.3356568>
- Huy H. Nguyen, Junichi Yamagishi, and Isao Echizen. 2019. Capsule-forensics: Using Capsule Networks to Detect Forged Images and Videos. In *ICASSP 2019 - 2019 IEEE International Conference on Acoustics, Speech and Signal Processing (ICASSP)*, 2307–2311.
- Hoang Mark Nguyen and Reza Derakhshani. 2020. Eyebrow Recognition for Identifying Deepfake Videos. In *2020 International Conference of the Biometrics Special Interest Group (BIOSIG)*, 1–5.
- Michael J Reale, Peng Liu, Lijun Yin, and Shaun Canavan. 2013. Art critic: Multisignal vision and speech interaction system in a gaming context. *IEEE transactions on cybernetics* 43, 6 (2013), 1546–1559.
- Andreas Rossler, Davide Cozzolino, Luisa Verdoliva, Christian Riess, Justus Thies, and Matthias Niessner. 2019. FaceForensics++: Learning to Detect Manipulated Facial Images. In *The IEEE International Conference on Computer Vision (ICCV)*.
- Aniket Roy, Diangarti Bhalang Tarian, Rajat Subhra Chakraborty, and Ruchira Naskar. 2018. Discrete Cosine Transform Residual Feature Based Filtering Forgery and Splicing Detection in JPEG Images. In *The IEEE Conference on Computer Vision and Pattern Recognition (CVPR) Workshops*.
- Shunsuke Saito, Lingyu Wei, Liwen Hu, Koki Nagano, and Hao Li. 2017. Photorealistic Facial Texture Inference Using Deep Neural Networks. *2017 IEEE Conference on Computer Vision and Pattern Recognition (CVPR)* (2017), 2326–2335.
- Thiago Santini, Wolfgang Fuhl, and Enkelejd Kasneci. 2018. PuReST: Robust Pupil Tracking for Real-Time Pervasive Eye Tracking. In *Proceedings of the 2018 ACM Symposium on Eye Tracking Research & Applications (Warsaw, Poland) (ETRA '18)*. Association for Computing Machinery, New York, NY, USA, Article 61, 5 pages. <https://doi.org/10.1145/3204493.3204578>
- Christian Szegedy, Vincent Vanhoucke, Sergey Ioffe, Jon Shlens, and Zbigniew Wojna. 2016. Rethinking the Inception Architecture for Computer Vision. In *IEEE Conf. on Computer Vision and Pattern Recognition (CVPR)*.
- Shahroz Tariq, Sangyup Lee, Hoyoung Kim, Youjin Shin, and Simon S. Woo. 2018. Detecting Both Machine and Human Created Fake Face Images in the Wild. In *Proceedings of the 2Nd International Workshop on Multimedia Privacy and Security (Toronto, Canada) (MPS '18)*. ACM, New York, NY, USA, 81–87.
- Justus Thies, Michael Zollhöfer, and Matthias Nießner. 2019. Deferred Neural Rendering: Image Synthesis Using Neural Textures. *ACM Trans. Graph.* 38, 4, Article 66 (July 2019), 12 pages. <https://doi.org/10.1145/3306346.3323035>
- Justus Thies, Michael Zollhofer, Marc Stamminger, Christian Theobalt, and Matthias Nießner. 2016. Face2Face: Real-time Face Capture and Reenactment of RGB Videos. In *Proc. Computer Vision and Pattern Recognition (CVPR)*, IEEE.
- Justus Thies, Michael Zollhofer, Marc Stamminger, Christian Theobalt, and Matthias Niessner. 2018. FaceVR: Real-Time Gaze-Aware Facial Reenactment in Virtual Reality. *ACM Trans. Graph.* 37, 2, Article 25 (June 2018), 15 pages.
- Ting-Chun Wang, Ming-Yu Liu, Jun-Yan Zhu, Guilin Liu, Andrew Tao, Jan Kautz, and Bryan Catanzaro. 2018. Video-to-Video Synthesis. In *Advances in Neural Information Processing Systems (NIPS)*.
- Erroll Wood, Tadas Baltruaitis, Xucong Zhang, Yusuke Sugano, Peter Robinson, and Andreas Bulling. 2015. Rendering of Eyes for Eye-Shape Registration and Gaze Estimation. In *Proceedings of the 2015 IEEE International Conference on Computer Vision (ICCV) (ICCV '15)*. IEEE Computer Society, USA, 3756?3764. <https://doi.org/10.1109/ICCV.2015.428>
- Xin Yang, Yuezun Li, and Siwei Lyu. 2019. Exposing Deep Fakes Using Inconsistent Head Poses. In *IEEE International Conference on Acoustics, Speech and Signal Processing (ICASSP)*, 8261–8265.
- Xucong Zhang, Yusuke Sugano, Mario Fritz, and Andreas Bulling. 2019. MPIIGaze: Real-World Dataset and Deep Appearance-Based Gaze Estimation. *IEEE Transactions on Pattern Analysis and Machine Intelligence* 41, 1 (2019), 162–175. <https://doi.org/10.1109/TPAMI.2017.2778103>
- Ying Zhang, Lilei Zheng, and Vrizzlynn LL Thing. 2017. Automated face swapping and its detection. In *2017 IEEE 2nd International Conference on Signal and Image*

Processing (ICSIIP), 15–19. <https://doi.org/10.1109/SIPROCESS.2017.8124497>
 Peng Zhou, Xintong Han, Vlad I Morariu, and Larry S Davis. 2017. Two-Stream Neural Networks for Tampered Face Detection. In *2017 IEEE Conference on Computer Vision and Pattern Recognition Workshops (CVPRW)*. 1831–1839. <https://doi.org/10.1109/CVPRW.2017.229>
 Piotr Zieliski. 2007. Opengazer: open-source gaze tracker for ordinary webcams. <http://www.inference.phy.cam.ac.uk/opengazer/>.

A SIGNATURE COMPOSITION

In Table 7, we list elements of our input tensor (i.e., the signature) that collates the spectral and temporal versions of the aforementioned visual, geometric, and metric features. SS means “shift by min+scale by max” and d^+ corresponds to maximum IPD. Multiple features occupying one row corresponds to features being merged into a three channel value. Channels with stars (*) indicate that a single channel value is duplicated into multiple channels per its importance. Cross correlation features intake double signals and output single signals. The signatures include 24 visual, 24* geometric, and 12 metric features. Finally, all $|T| = 20 \times 3 \times \omega$ values are transformed and resized to the spectral domain, creating $|S| = 20 \times 3 \times \omega$ values, constituting the $40 \times \omega \times 3$ size signatures.

Table 7: Signatures. We enlist the elements, their parts, sides, channels, and normalizations that make up our fake and real signatures.

Set	Feature	Part	Side	Chan.	Norm.
Visual	Color	Iris	Left	3	/256
Visual	Color	Iris	Right	3	/256
Visual	Color	Pupil	Left	3	/256
Visual	Color	Pupil	Right	3	/256
Visual	Area	Eye	Left	1	SS
Visual	Area	Eye	Right	1	SS
Geometric	Area	Eye	Left-Right	1	/ d^+
Visual	Area	Iris	Left	1	SS
Visual	Area	Iris	Right	1	SS
Geometric	Area	Iris	Left-Right	1	SS
Visual	Area	Pupil	Left	1	SS
Visual	Area	Pupil	Right	1	SS
Geometric	Area	Pupil	Left-Right	1	/ $d^+ - 1$
Visual	Color	Iris	Left-Right	3	/256
Visual	Color	Pupil	Left-Right	3	/256
Geometric	Vector	Gaze	Left	3	SS2
Geometric	Vector	Gaze	Right	3	SS2
Geometric	Point	Gaze	-	3	SS
Geometric	Error	Gaze	-	3	/ d^+
Geometric	Cost	Gaze	-	3*	SS
Geometric	Distance	Eye	-	3*	SS
Geometric	Distance	Pupil	-	3*	SS
Cross	Color	Iris	Both	2x3 > 3	SS
Cross	Color	Pupil	Both	2x3 > 3	SS
Cross	Area	Iris	Both	2 > 1	SS
Cross	Area	Pupil	Both	2 > 1	SS
Cross	Area	Eye	Both	2 > 1	SS
Cross	Vector	Gaze	Both	2x3 > 3	SS

B NETWORK LAYERS

We log our network layers, their arguments, and their output shapes in Table 8. Note that the order of layers and the network architecture are finalized empirically and theoretically [Han et al. 2017; Li et al. 2019]. We would also like to note that the main motivation of our paper is to analyze eye and gaze behavior of various deep fakes, and this simple but strong network is a part of the verification process for our findings. For production-level accuracies, we encourage researchers to invest in neural architecture search for building better alternatives utilizing our eye and gaze features.

Table 8: Network Layers. We document sizes, arguments, and outputs of each layer in our network.

Layer	Arguments	Output
Signature	-	40x64x3
Flatten	-	7680x1x1
Batch Norm	-	7680
Dense	256	256
Batch Norm	-	256
Leaky ReLu	0.2	256
Dropout	0.3	256
Dense	128	128
Batch Norm	-	128
Leaky ReLu	0.2	128
Dropout	0.3	128
Dense	64	64
Dense	2	2
Sigmoid	-	2